2024 IEEE 63rd Conference on Decision and Control (CDC)
December 16-19, 2024. MiCo, Milan, Italy

Robust control design for thruster driven Autonomous Underwater Vehicle

Diwakar Gurung[1] Vidit Gedam[1] Swapnil Laxman Jagadale[2] C S Kumar[1] Vishwanath Nagarajan[2]

***Abstract*— The paper presents a robust control strategy for an autonomous underwater vehicle (AUV) based on uncertainty and disturbance estimation (UDE) theory. A robust control design is essential for underwater vehicles due to their highly nonlinear dynamics and the presence of external disturbances. A α-UDE based control design has been formulated for the pitch and depth control of an axisymmetric testbed AUV that is entirely controlled by thrusters. Here, the first-order α-filter is used to estimate the uncertainties and disturbance alongside a feedback control law based on feedback linearization (FL) approach. We present the comparative numerical simulations to show the effectiveness of the proposed control system.**

***Index Terms*— Autonomous underwater vehicle, Thruster, Robust control, α-filter.**

I. INTRODUCTION

Autonomous underwater vehicles (AUVs) are unmanned, self-propelled vehicles that operate underwater without direct human control. AUVs have a wide range of applications across various industries and research areas, including oceanography, underwater pipeline and infrastructure inspection, defense, and security. Thruster driven AUVs are fully operated by thrusters and have higher maneuverability for low-speed tasks and hovering operations [1], [2], [3]. AUVs are highly nonlinear systems, and their dynamics are known to be coupled. Moreover, operating an AUV becomes difficult in adverse conditions due to model uncertainties and external disturbances, such as ocean waves. AUVs require a robust control strategy to achieve the desired motion. In the context of thruster driven AUVs, only thrusters are used to regulate various different sub-operations of maneuvering, like forward speed control, steering control, and diving.

The existing literature has formulated various control strategies to address the AUV control problem. A PID-based control strategy is implemented for position and orientation control, as reported in [3], [4], [5]. A backstepping control strategy had been implemented in [6] and [7] for the path following of AUV. To provide robustness against uncertain dynamics and external disturbances, sliding mode control (SMC) and time delay estimation (TDE)-based control strategies have been used for the trajectory control of the AUVs, as given in [8], [9], [10], [11]. With the advent of more powerful digital onboard computers, intelligent control methods based on fuzzy logic and artificial neural networks have been successfully implemented in underwater vehicle applications, as presented in [12], [13], [14]. Intelligent control strategies are either used to estimate the unmodeled dynamics and external disturbances directly or used as an intelligent adaptive mechanism to auto-tune the controller parameters subjected to the changing dynamics. An observation-based control approach based on uncertainty and disturbance estimation theory can be implemented for the AUV motion control [15]. The control strategy utilizes various filter types to estimate the uncertainty in the system's dynamics alongside a feedback control law [16]. Because of its simple design, UDE-based control can be a beneficial choice for marine vehicle operation. UDE-based control has been implemented for surface vessels and ships in [17], [18], [19]. The present study investigates the application of α-UDE-based control design for the pitch and depth control of an AUV fully operated by thrusters. Here, we use a first-order α-filter formulated by Kuperman [20] to estimate uncertainty and external disturbances, which is combined with a feedback control law based on the feedback linearization method to control the AUV.

The paper is organised as follows: The mathematical model of an experimental testbed AUV, along with the four-quadrant propulsion model of the thruster, is presented in Section II. In Section III, the UDE-based control design is derived based on a first-order α-filter for the control of the testbed AUV. Section IV discusses the numerical simulation outputs. Section V presents the concluding remarks.

II. AUV MODEL

Fig. 1. Thruster driven testbed AUV developed by IIT Kharagpur [2].

The proposed control strategy in the present work is tested for an experimental testbed AUV (see Fig. 1) developed by the Robotics and Intelligent Systems Laboratory at Indian Institute of Technology Kharagpur, India. The AUV is entirely operated by five identical thrusters manufactured by Tecnadyne [21]. It has one main thruster at the stern end and two vertical and two side horizontal thrusters that are fitted through the body. The vertical thrusters are operated simultaneously to control the depth and pitch by differential thrusting.

[1]Department of Mechanical Engineering, Indian Institute of Technology Kharagpur, India.
[2]Department of Ocean Engineering and Naval Architecture, Indian Institute of Technology Kharagpur, India.

A. Reference frames and kinematics

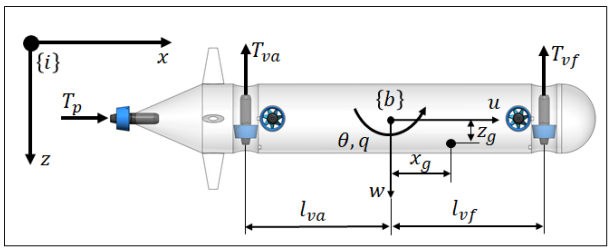

Fig. 2. AUV reference frame.

The vehicle's position and velocity are described using the inertial frame $\{i\}$ and the body frame $\{b\}$, as shown in Fig. 2. The position and orientation of the vehicle are represented by the vector $\eta = [x, z, \theta]^T$ in $\{i\}$-frame, while the vehicle body velocity is represented by the vector $\nu = [u, w, q]^T$ in $\{b\}$-frame. The kinematic relationship between the AUV velocities in inertial and body frames is expressed by Eq. 1.

$$\dot{\eta} = J(\theta)\nu \tag{1}$$

Where $J(\theta)$ is the transformation matrix and is defined by Eq. 2.

$$J(\theta) = \begin{bmatrix} \cos(\theta) & \sin(\theta) & 0 \\ -\sin(\theta) & \cos(\theta) & 0 \\ 0 & 0 & 1 \end{bmatrix} \tag{2}$$

B. Dynamics

The dynamic model of the testbed AUV in a vertical plane is defined by Eq. 3.

$$M\dot{\nu} + C(\nu)\nu + D(\nu)\nu + g(\eta) = \tau_T + d(t) \tag{3}$$

Here, M and $C(\nu)$ represent the inertial and Coriolis-centripetal matrix, respectively. These matrices include both the rigid body inertia and hydrodynamic added mass and are defined by equations 4 and 5.

$$M = \begin{bmatrix} m - X_{\dot{u}} & 0 & mz_g \\ 0 & m - Z_{\dot{w}} & -mx_g - Z_{\dot{q}} \\ mz_g & -mx_g - M_{\dot{w}} & I_{yy} - M_{\dot{q}} \end{bmatrix} \tag{4}$$

$$C(\nu) = \begin{bmatrix} 0 & 0 & -m(x_g q - w) - Z_{\dot{w}} w \\ 0 & 0 & -m(z_g q + u) + X_{\dot{u}} u \\ m(x_g q - w) + Z_{\dot{w}} w & m(z_g q + u) - X_{\dot{u}} u & 0 \end{bmatrix} \tag{5}$$

Where m is the vehicle mass, and I_{yy} is the moment of inertia about the pitch axis. (x_g, z_g) is the position of the center of gravity and is measured along the axes of the $\{b\}$-frame. $X_{\dot{u}}$, $Z_{\dot{w}}$, $Z_{\dot{q}}$, $M_{\dot{w}}$, and $M_{\dot{q}}$ represent the added inertia. $D(\nu)$ represents the hydrodynamic damping coefficient matrix and is modeled according to Eq. 6.

$$D(\nu) = \begin{bmatrix} X_u + X_{|u|u}|u| & 0 & 0 \\ 0 & Z_w + Z_{|w|w}|w| & Z_q + Z_{|q|q}|q| \\ 0 & M_w + M_{|w|w}|w| & M_q + M_{|q|q}|q| \end{bmatrix} \tag{6}$$

$g(\eta)$ defines the restoring forces and moments vector due to gravity and buoyancy and is expressed by Eq. 7.

$$g(\eta) = \begin{bmatrix} (W - B)\sin(\theta) \\ -(W - B)\cos(\theta) \\ (z_g W - z_b B)\sin(\theta) + (x_g W - x_b B)\cos(\theta) \end{bmatrix} \tag{7}$$

Here, W and B represents the AUV weight and buoyancy, respectively. (x_b, z_b) denotes the position of center of buoyancy and is measured along the body frame axes. The vector $d(t) = [d_x(t), d_z(t), d_\theta(t)]^T$ represents the lumped disturbance which combines the vehicle unmodeled dynamics and external disturbances acting on the AUV. τ_T represents the control forces input vector, which corresponds to the forces and moments generated by thrusters and is modeled as shown in Eq. 8.

$$\tau_T = \begin{bmatrix} \tau_{surge} \\ \tau_{depth} \\ \tau_{pitch} \end{bmatrix} = \begin{bmatrix} 1 & 0 & 0 \\ 0 & -1 & -1 \\ 0 & l_{vf} & l_{va} \end{bmatrix} \begin{bmatrix} T_p \\ T_{vf} \\ T_{va} \end{bmatrix} \tag{8}$$

T_p, T_{vf}, and T_{va} denote the thrust generated by main propulsion and two vertical thrusters, respectively. Note that the heave force (τ_{depth}) required for depth control and pitch moment (τ_{pitch}) required for pitch control are produced using the differential thrust of two vertical thrusters. l_{vf} and l_{va} represent the vertical thruster moment arm lengths.

C. Four quadrant propeller model

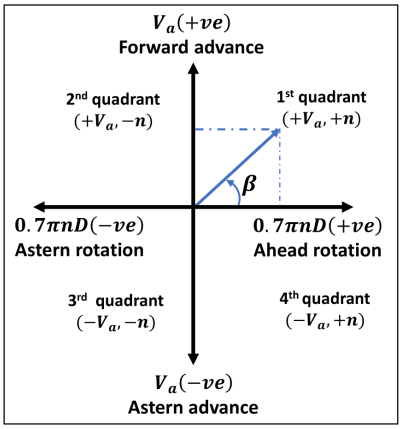

Fig. 3. Thruster four quadrant notation.

To identify the relationship between the propeller's rotational speed and its resulting thrust force and torque, a four-quadrant propulsion model is defined. Referring to Fig. 3, the four-quadrant notation represents the different propeller operating states based on the direction of propeller rotational speed (n) and advancing velocity (V_a) inside the fluid. The operational state is defined by an advance angle β as expressed by Eq. 9.

$$\beta = \tan^{-1}\left(\frac{V_a}{0.7\pi nD}\right) \tag{9}$$

Where D is the propeller diameter. The thrust force T and torque Q are expressed by equations 10 and 11, respectively.

$$T = C_T^*(\beta)\frac{\pi}{8}\rho[V_a^2 + (0.7n\pi D)^2]D^2 \tag{10}$$

$$Q = C_Q^*(\beta)\frac{\pi}{8}\rho[V_a^2 + (0.7n\pi D)^2]D^3 \quad (11)$$

$C_T^*(\beta)$ and $C_Q^*(\beta)$ are the non-dimensional thrust coefficient and torque coefficient, respectively. These coefficients are evaluated as a function of the advance angle β, which covers all four quadrants. Both $C_T^*(\beta)$ and $C_Q^*(\beta)$ possess periodicity within the interval of $0^o \leq \beta \leq 360^o$ and can be represented through Fourier series approximation as given in Eq. 12.

$$C_i^*(\beta) = \sum_{k=0}^{20}(A_i(k)\cos(k\beta) + B_i(k)\sin(k\beta)), i = T, Q \quad (12)$$

$A_T(k)$, $B_T(k)$, $A_Q(k)$, and $B_Q(k)$ are the fourier coefficients. Note that the advance velocity for the main propulsion thruster and vertical thrusters are defined according to its position and orientation with respect to the body origin. The advance velocity of the thrusters is given by Eq. 13.

$$V_p = u, V_{vf} = -w + l_{vf}q, V_{va} = -w - l_{va}q \quad (13)$$

The thruster's rotational speed is denoted by n_p, n_{vf}, and n_{va}. For the present testbed AUV thrusters, we assume the propeller model of Ka 4-70 with a 19A nozzle and feed it into the numerical simulation. The corresponding sets of fourier coefficients for Ka 4-70 propeller are provided in [22].

III. Control system design

This section formulates the UDE-based control system using a first-order α-filter for the depth and pitch control of the testbed AUV. Without the loss of generality, the vehicle dynamics defined by Eq. 3 is rewritten in inertial frame according to Eq. 14.

$$\ddot{\eta} = \dot{J}(\theta)\nu + J(\theta)M^{-1}[-C(\nu)\nu - D(\nu)\nu - g(\eta) + \tau_T + d(t)] \quad (14)$$

Let the vector $\eta_d = [x_d, z_d, \theta_d]^T$ defines the desired position, and the vector $\tilde{\eta} = (\eta_d - \eta)$ indicates the position tracking error. Initially, a nominal feedback control law based on feedback linearization is formulated considering the known vehicle dynamics as expressed by Eq. 15.

$$\tau_T = \Lambda + M_\theta U(t) \quad (15)$$

Where, $M_\theta = MJ^{-1}(\theta)$ and $\Lambda = M_\theta(\theta)\dot{J}(\theta)\nu + C(\nu)\nu + D(\nu)\nu + g(\eta)$. $U(t)$ represents the commanded acceleration vector and is expressed by Eq. 16.

$$U_i(t) = \ddot{\eta}_{di} + k_{di}\dot{\tilde{\eta}}_i + k_{pi}\tilde{\eta}_i, i = x, z, \theta \quad (16)$$

Implementing the control law given by equations 15 and 16 and assuming no lumped disturbance, i.e., $d(t) = 0$, the position tracking error dynamics for x, z and θ lead to Eq. 17.

$$\ddot{\tilde{\eta}}_i + k_{di}\dot{\tilde{\eta}}_i + k_{pi}\tilde{\eta}_i = 0 \quad (17)$$

The feedback control gains k_{di} and k_{pi} are chosen to ensure the stability of the error dynamics as described by Eq. 17. The feedback linearization (FL)-based control design tends to show good tracking performance for the known system dynamics with no lumped disturbances. However, this condition is seldom met for underwater vehicles. To compensate for the model uncertainties and external disturbances, first-order α-filter is utilised to estimate the lumped disturbance [23]. The feedback control law based on feedback linearization method given by Eq. 15 is modified as shown in Eq. 18.

$$\tau_T = \Lambda + M_\theta[U(t) - \hat{d}(t)] \quad (18)$$

Where the term $\hat{d}(t) = [\hat{d}_x(t), \hat{d}_z(t), \hat{d}_\theta(t)]^T$ defines the estimate of the lumped disturbance defined by $d(t)$. Implementing the control law by Eq. 18, the system dynamics given by Eq. 14 reduces to Eq. 19.

$$\ddot{\eta}_i = d_i(t) - \hat{d}_i(t) + U_i(t) \quad (19)$$

The estimate based on first-order α-filter is defined according to Eq. 20.

$$\hat{d}_i(s) = G_{fi}(s)d_i(s) \quad (20)$$

Where,

$$G_{fi}(s) = \frac{(1-\alpha_{di})\tau_{di}s + 1}{1 + \tau_{di}s} \quad (21)$$

Here, α_d and τ_d are the parameters of α-filter. Eq. 20 is rewritten in time domain as shown in Eq. 22.

$$\hat{d}_i(t) + \tau_{di}\dot{\hat{d}}_i(t) = (1-\alpha_{di})\tau_{di}\dot{d}_i(t) + d_i(t) \quad (22)$$

The derivation of Eq. 19 leads to Eq. 23.

$$\dddot{\eta}_i = \dot{d}_i(t) - \dot{\hat{d}}_i(t) + \dot{U}_i(t) \quad (23)$$

Combining equations 22 and 23 and taking the integral, the disturbance estimate expression is obtained as given by Eq. 24.

$$\hat{d}_i = \frac{(1-\alpha_{di})}{\alpha_{di}}(\ddot{\eta}_i - U_i(t)) + \frac{1}{\alpha_{di}\tau_{di}}\dot{\eta}_i - \frac{1}{\alpha_{di}\tau_{di}}\int U_i(t)dt \quad (24)$$

The tracking error dynamics previously given by Eq. 17 is modified according to Eq. 25.

$$\ddot{\tilde{\eta}}_i + K_d\dot{\tilde{\eta}}_i + K_p\tilde{\eta}_i = \tilde{d}_i \quad (25)$$

Where $\tilde{d}_i = d_i(t) - \hat{d}_i(t)$ is the disturbance estimation error. Note that the disturbance estimation error and its dynamics have a significant impact on the tracking error's stability. Appropriate selection of controller gains and filter time constants can ensure the closed-loop stability of the overall system. The disturbance estimation error dynamics is given by Eq. 26.

$$\dot{\tilde{d}}_i = -\frac{1}{\tau_{di}}\tilde{d}_i + \alpha_i\dot{d}_i \quad (26)$$

By selecting $\tau_{di} > 0$ and smaller value for α_{di}, the disturbance estimation error remains bounded for bounded values of $|d_i(t)|$ and $|\dot{d}_i(t)|$. If $\dot{d}_i = 0$, $\tilde{d}_i$ will asymptotically converge to zero.

The present work mainly focuses on regulating the vehicle's depth (z) and pitch (θ), while the x-position remains free. The control input τ_{depth} and τ_{pitch} are obtained as per the control law given by Eq. 18. The control input can be mapped according to Eq. 8 to get the individual vertical thruster forces. The performance of the α-UDE based control design given by Eq. 18 is compared with the FL-based control design given by Eq. 15 through the numerical simulation.

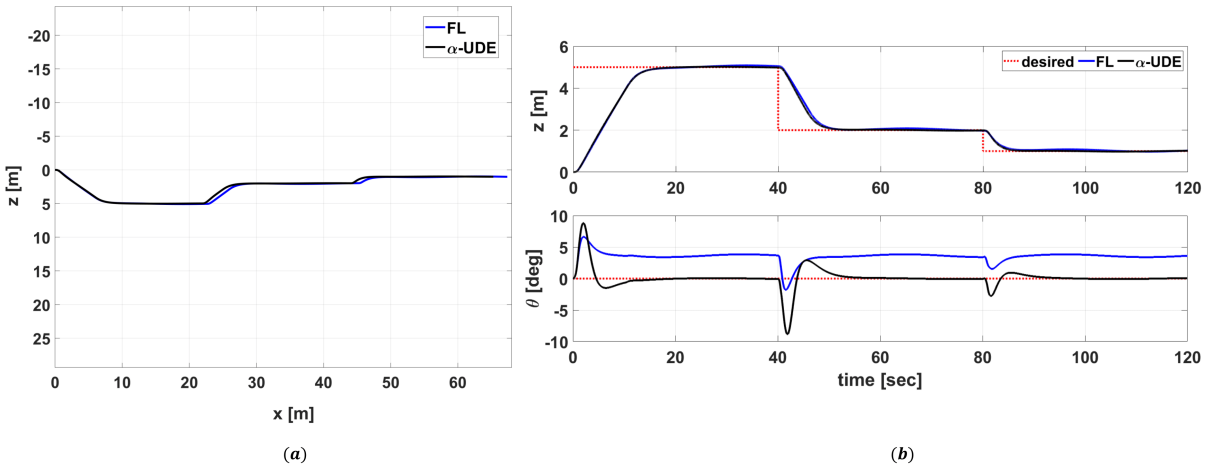

(a) (b)

Fig. 4. (a) Trajectory of testbed AUV in X-Z plane (b) Simulation results for a comparison of depth and pitch tracking under feedback linearisation and α-UDE based control design.

IV. Simulation Results and Discussions

This section presents the results of the maneuvering simulation carried out for the testbed AUV's depth and pitch control scenarios. The simulation is executed using both the nominal FL-based control design and the α-UDE based control design. The simulation utilizes the dynamic model established in Section II, and the model parameters specified in Table II are tuned in the simulation configuration. The simulation follows the Runge-Kutta method, with a step size of 0.01 seconds. We assume full state feedback throughout the entire simulation, which is executed for 120 seconds. The vehicle is commanded to track the depth and pitch reference values given by Eq. 27.

$$z_d(t) = \begin{cases} 5m, & 0 \leq t < 40 \\ 2m, & 40 \leq t < 80 \\ 1m, & 80 \leq t \leq 120 \end{cases} \tag{27}$$

$$\theta_d(t) = 0^o, 0 \leq t \leq 120 \tag{28}$$

The disturbances provided in the simulation are expressed by Eq. 29.

$$d_x(t) = 0\,N, d_z(t) = 5 + 10\cos(0.2t)\,N, d_\theta(t) = 2\,N.m \tag{29}$$

The control feedback gain values for both the control designs are selected as shown in Eq. 30.

$$k_{pz} = 1, k_{dz} = 2.5, k_{p\theta} = 1, k_{d\theta} = 2 \tag{30}$$

The parameters of the filter used in α-UDE based control design are selected as shown in Eq. 31.

$$\tau_{dz} = 2.5, \tau_{d\theta} = 2.5, \alpha_{dz} = 0.9, \alpha_{d\theta} = 0.85 \tag{31}$$

The main propulsion thruster is provided with a constant rotational speed value of 12.5 rev/sec, allowing the AUV to move forward at a certain speed. Figure 4(a) shows the vehicle's trajectory in the vertical plane. The pitch and depth responses are shown in Fig. 4(b), which depicts better tracking performance of α-UDE based control design compared to FL in the presence of external disturbances. Furthermore, the FL-based control design shows a significant steady-state error in pitch, whereas α-UDE maintains the desired pitch angle but overshoots in the initial phase of the reference value change. Figure 5 exhibits the vehicle velocity response, and it can be observed that the forward surge velocity of around 1 knot is achieved. Figure 7 shows the disturbance estimate in α-UDE control design, implying that the proposed estimation law based on α-filter is able to effectively observe the disturbance. The control inputs τ_{depth} and τ_{pitch} are shown in Figs. 6(a) and 6(b) and the corresponding vertical thruster forces and propeller rotational

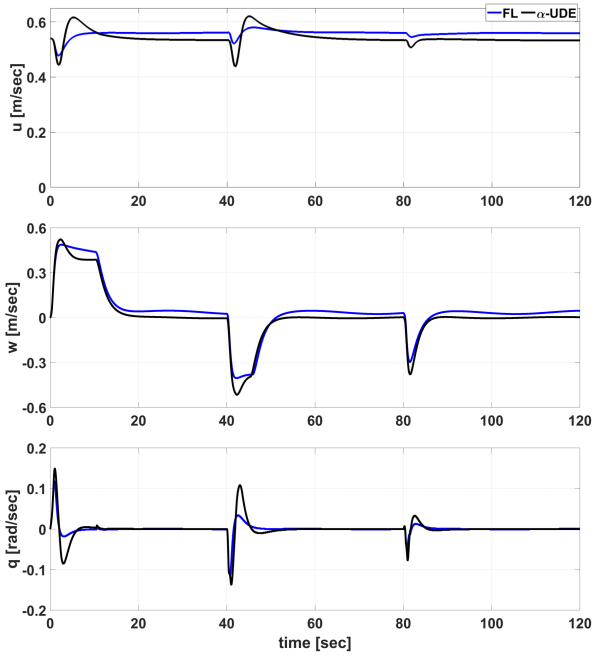

Fig. 5. Simulation results for the linear and angular velocity responses of the testbed AUV.

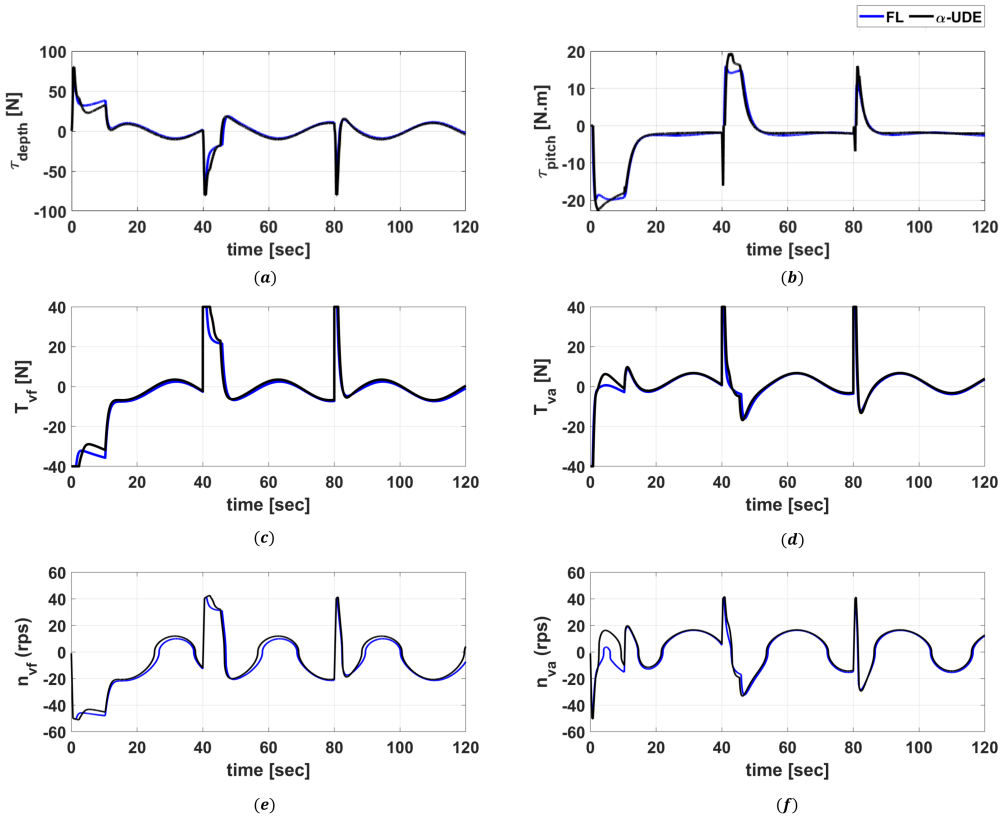

Fig. 6. Control force inputs (τ_{depth},τ_{pitch}) and the corresponding thrust forces (T_{vf},T_{va}) and rotational speeds (n_{vf},n_{va}) of the vertical thrusters.

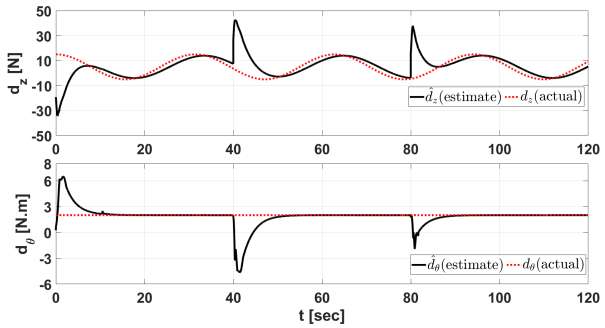

Fig. 7. Simulation results for estimation of disturbance by first-order α-filter in heave and pitch direction.

speeds are shown in Figs. 6(c)-(f). Note that the thrust demand is initially high due to the large initial error for both the control design and also the disturbance estimate value obtained in the case of the α-UDE based control design. The tracking performance can be quantitatively measured by the performance index as given by Eq. 32.

$$J_E = J_z + J_\theta, J_z = \int |z_d - z| dt, J_\theta = \int \frac{180}{\pi} |\theta_d - \theta| dt \quad (32)$$

Here, J_E denotes the tracking performance quantified by the integral of the absolute values of the pitch and depth tracking errors. The performance related to control effort can be quantified by the total energy expended by the thrusters during maneuvering. The propeller torque and power requirement are evaluated using the four-quadrant model, as discussed in Section II-C. The total energy consumed (E_{total}) is expressed by Eq. 33.

$$E_{total} = \int (2\pi n_p Q_p + 2\pi n_{vf} Q_{vf} + 2\pi n_{va} Q_{va}) dt \quad (33)$$

The performance index and energy consumption values for both FL and α-UDE based control design are given in Table I. The α-UDE has a minimum index value compared to FL-based control design owing to the better tracking performance of the α-UDE based control design. Moreover, the energy consumption for both control designs is nearly comparable. By adjusting the filter parameters according to the performance index for various maneuvering conditions, we can enhance the performance of the UDE-based control design for the AUV control.

TABLE I

PERFORMANCE INDEX AND ENERGY CONSUMPTION FOR FL AND α-UDE BASED CONTROL DESIGN.

	J_θ	J_z	J_E	$E_{total}(Kwatt.sec)$
FL	423.055	55.613	478.669	318.816
α-UDE	73.436	51.328	124.764	323.820

V. Conclusion

In this paper, a α-UDE based robust control design is formulated and implemented for the pitch and depth control of a thruster-driven autonomous underwater vehicle. This control scheme consists of a nominal feedback control law based on feedback linearization, augmented by an estimation algorithm that utilizes a first-order α filter to estimate the uncertainties and disturbances acting on the vehicle. The performance of the proposed control design is verified through numerical simulation and is compared with the FL-based control design. The four-quadrant propulsion model of the thruster is also included in the maneuvering simulation. We observe that the α-UDE based control design effectively tracks the desired trajectory of the testbed AUV and provides robustness against external disturbances. We can further improve and optimize the performance of the UDE-based control design by tuning the filter parameters based on performance index for different maneuvering conditions. Future work will include the experimental verification of the proposed control system.

References

[1] M. Carreras, J. D. Hernández, E. Vidal, N. Palomeras, D. Ribas, and P. Ridao, "Sparus ii auv—a hovering vehicle for seabed inspection," *IEEE Journal of Oceanic Engineering*, vol. 43, no. 2, pp. 344–355, 2018.

[2] R. Kumar, C. Kumar, D. Sen, and A. Dasgupta, "Discrete time-delay control of an autonomous underwater vehicle: Theory and experimental results," *Ocean engineering*, vol. 36, no. 1, pp. 74–81, 2009.

[3] T. Matsuda, R. Takizawa, T. Sakamaki, and T. Maki, "Landing method of autonomous underwater vehicles for seafloor surveying," *Applied Ocean Research*, vol. 101, p. 102221, 2020.

[4] P. V. Patil, M. K. Khan, M. Korulla, V. Nagarajan, and O. P. Sha, "Design optimization of an auv for performing depth control maneuver," *Ocean Engineering*, vol. 266, p. 112929, 2022.

[5] D. Gurung, C. S. Kumar, and V. Nagarajan, "2023a-os4-8 motion control of a thruster driven autonomous underwater vehicle," in *Conference Proceedings The Japan Society of Naval Architects and Ocean Engineers 37*. The Japan Society of Naval Architects and Ocean Engineers, 2023, pp. 207–213.

[6] X. Xiang, L. Lapierre, and B. Jouvencel, "Smooth transition of auv motion control: From fully-actuated to under-actuated configuration," *Robotics and Autonomous Systems*, vol. 67, pp. 14–22, 2015.

[7] K. D. Do, J. Pan, and Z.-P. Jiang, "Robust and adaptive path following for underactuated autonomous underwater vehicles," *Ocean Engineering*, vol. 31, no. 16, pp. 1967–1997, 2004.

[8] A. J. Healey and D. Lienard, "Multivariable sliding mode control for autonomous diving and steering of unmanned underwater vehicles," *IEEE journal of Oceanic Engineering*, vol. 18, no. 3, pp. 327–339, 1993.

[9] K. Tanakitkorn, P. A. Wilson, S. R. Turnock, and A. B. Phillips, "Sliding mode heading control of an overactuated, hover-capable autonomous underwater vehicle with experimental verification," *Journal of Field Robotics*, vol. 35, no. 3, pp. 396–415, 2018.

[10] D. Gurung, C. Kumar, and V. Nagarajan, "Robust path following control of autonomous underwater vehicle using combined time delay estimation and backstepping method," in *Recent Advances in Machines and Mechanisms: Select Proceedings of the iNaCoMM 2021*. Springer, 2022, pp. 587–599.

[11] J. Guerrero, A. Chemori, J. Torres, and V. Creuze, "Time-delay high-order sliding mode control for trajectory tracking of autonomous underwater vehicles under disturbances," *Ocean Engineering*, vol. 268, p. 113375, 2023.

[12] Y. Chen, R. Zhang, X. Zhao, and J. Gao, "Tracking control of underwater vehicle subject to uncertainties using fuzzy inverse desired trajectory compensation technique," *Journal of Marine Science and Technology*, vol. 21, pp. 624–650, 2016.

[13] M. W. Hasan and N. H. Abbas, "Disturbance rejection for underwater robotic vehicle based on adaptive fuzzy with nonlinear pid controller," *ISA transactions*, vol. 130, pp. 360–376, 2022.

[14] B. Seok Park, "Neural network-based tracking control of underactuated autonomous underwater vehicles with model uncertainties," *Journal of dynamic systems, measurement, and control*, vol. 137, no. 2, p. 021004, 2015.

[15] D. Gurung, C. S. Kumar, and V. Nagarajan, "Extended state observer-based control of underactuated autonomous underwater vehicle in a vertical plane," in *International Conference on Industrial Problems on Machines and Mechanism*. Springer, 2022, pp. 83–90.

[16] T. Chandar and S. Talole, "Improving the performance of ude-based controller using a new filter design," *Nonlinear Dynamics*, vol. 77, no. 3, pp. 753–768, 2014.

[17] S. He, S.-L. Dai, Z. Zhao, and T. Zou, "Uncertainty and disturbance estimator-based distributed synchronization control for multiple marine surface vehicles with prescribed performance," *Ocean Engineering*, vol. 261, p. 111867, 2022.

[18] A. Bhatt, S. Das, and S. Talole, "Robust backstepping ship autopilot design," *Journal of Marine Engineering & Technology*, vol. 20, no. 1, pp. 34–41, 2021.

[19] C. Hu, D. Wu, Y. Liao, and X. Hu, "Sliding mode control unified with the uncertainty and disturbance estimator for dynamically positioned vessels subjected to uncertainties and unknown disturbances," *Applied Ocean Research*, vol. 109, p. 102564, 2021.

[20] A. Kuperman, "Design of α-filter-based ude controllers considering finite control bandwidth," *Nonlinear Dynamics*, vol. 81, no. 1, pp. 411–416, 2015.

[21] https://tecnadyne.com, accessed on 2024-09-09.

[22] J. Carlton, *Marine propellers and propulsion*.

[23] Q.-C. Zhong and D. Rees, "Control of uncertain lti systems based on an uncertainty and disturbance estimator," *J. Dyn. Sys., Meas., Control*, vol. 126, no. 4, pp. 905–910, 2004.

Appendix

TABLE II

AUV testbed dynamic model parameters.

Paramater	Description	Value	Unit
m	AUV mass	80.100	kg
W	Weight	780.870	N
B	Buoyancy	785.780	N
I_{yy}	Moment of Inertia	12.010	$kg.m^2$
(x_g, z_g)	Center of Gravity	(0,0.025)	m
(x_b, z_b)	Center of Buoyancy	(0,0)	m
D	Thruster propeller dia	0.073	m
(L_{vf}, L_{va})	Vertical thruster moment arm lengths	(0.585,-0.585)	m
$X_{\dot{u}}$	Added mass terms	-4.018	kg
$Z_{\dot{w}}$		-89.168	kg
$Z_{\dot{q}}$		0.240	$kg.m/rad$
$M_{\dot{w}}$		0.240	$kg.m$
$M_{\dot{q}}$		-19.560	$kg.m^2/rad$
X_u	Hydrodynamic damping terms	-0.230	kg/sec
$X_{\|u\|u}$		-8.070	kg/m
Z_w		-26.561	kg/sec
$Z_{\|w\|w}$		-119.456	kg/m
M_w		15.264	$kg.m/sec$
$M_{\|w\|w}$		-16.862	kg
Z_q		-2.848	$kg.m.sec/rad$
$Z_{\|q\|q}$		-290.363	$kg.m/rad^2$
M_q		-2.763	$kg.m^2.sec/rad$
$M_{\|q\|q}$		-252.996	$kg.m^2/rad^2$